Analytica Chimica Acta xxx (2017) 1–6

Contents lists available at ScienceDirect

Analytica Chimica Acta

journal homepage: www.elsevier.com/locate/aca

Plasmon-induced photoelectrochemical biosensor for *in situ* real-time measurement of biotin-streptavidin binding kinetics under visible light irradiation

Jingchun Guo [a], Tomoya Oshikiri [a], Kosei Ueno [a], Xu Shi [a], Hiroaki Misawa [a, b, *]

[a] Research Institute for Electronic Science, Hokkaido University, Sapporo 001-0021, Japan
[b] Department of Applied Chemistry & Institute of Molecular Science, National Chiao Tung University, Hsinchu 30010, Taiwan

HIGHLIGHTS

- A plasmon-induced visible light-responsive photoelectrochemical biosensor is developed and the system can be miniaturized.

GRAPHICAL ABSTRACT

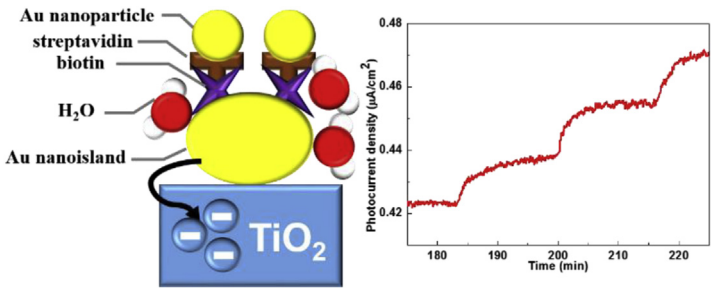

ARTICLE INFO

Article history:
Received 8 November 2016
Received in revised form
7 December 2016
Accepted 10 December 2016
Available online xxx

Keywords:
Photoelectrochemical biosensor
Localized surface plasmon
Kinetic analysis
Visible light-response

ABSTRACT

We developed a localized surface plasmon-induced visible light-responsive photoelectrochemical (PEC) biosensor using a titanium dioxide (TiO_2) photoelectrode loaded with gold nanoislands (AuNIs) for *in situ* real-time measurement of biotin-streptavidin association. As a proof of concept, self-assembled thiol-terminated biotin molecules bound on a AuNIs/TiO_2 photoelectrode were successfully utilized to explore the photocurrent response to streptavidin-modified gold nanoparticle (STA-AuNP) solutions. This plasmon-induced PEC biosensor is simple and easy to miniaturize. Additionally, the PEC biosensor achieves highly sensitive measurements under only visible light irradiation and prevents the UV-induced damage of samples. Furthermore, a novel approach has been proposed to realize the real-time monitoring of biotin-STA binding affinities and kinetics by analyzing the PEC sensing characteristics. This PEC biosensor and novel analysis method could provide a new approach for the specific electrical detection and real-time kinetic measurements for clinical diagnostics and drug development.

1. Introduction

Surface plasmon resonance (SPR) biosensors are primarily used as optical biosensors [1–3]. SPR involves the resonant oscillation of conduction electrons at a metal/dielectric interface excited by incident light, and the created charge density oscillations are referred to as surface plasmon polaritons (SPPs) [3]. The propagating SPPs have an electric field that exponentially decays into its surrounding medium with a penetration depth of several hundred nanometers [3]. Therefore, SPR biosensors possess an extremely high bulk dielectric sensitivity. However, several drawbacks limit

* Corresponding author. Research Institute for Electronic Science, Hokkaido University, Sapporo 001-0021, Japan.
E-mail address: misawa@es.hokudai.ac.jp (H. Misawa).

http://dx.doi.org/10.1016/j.aca.2016.12.025

the application of SPR biosensors. For example, the total apparatus becomes large because the optical system for measuring the incident angle dependence becomes complicated, and the spatial resolution is not small when using propagating SPPs, which in principle, restricts the measurement of multiple analytes. In addition, a fine temperature control unit is necessary because SPR is sensitive to refractive index changes [4]. When light is incident on sub-wavelength-sized metal nanoparticles, the excited collective oscillations of conduction electrons in the metallic nanoparticles form localized surface plasmon resonance (LSPR) [5–7]. LSPR biosensors are commonly utilized to detect biomolecular interactions through an optical response, such as LSPR spectral peak shifts [8,9] or change in extinction values [10,11]. The advantage of LSPR biosensors is their simplicity in optical setup compared to SPR sensors. However, real-time and highly sensitive measurements are difficult to achieve simultaneously due to the broad LSPR band, and ponderous instruments for optical measurements still limit its practical application. The fabrication of portable and miniaturized biosensors remains a challenge for optical biosensors.

Recently, a gold nanostructure-loaded titanium dioxide (TiO_2) system has received increased attention due to the LSPR-induced charge separation can improve the photoactivity of TiO_2 from the UV region to the visible and near infrared region [12–17]. The visible and near infrared photocurrent generations have been attributed to LSPR-induced charge separation following a hot-electron transfer from the gold nanostructure to the conduction band of TiO_2 [14]. Importantly, this photocurrent generation is induced by water oxidation. Therefore, water molecules are used as an electron source for photocurrent generation [15,16]. This behavior opens up a new horizon for applications in photocatalytic [18–20] and organic pollution degradation [21] utilizing visible light via LSPR-induced charge separation. If the biomolecular interactions occur on the surface of gold nanostructures, the photoelectrochemical (PEC) property should be modulated because the hot-electron transfer from the gold nanostructures to TiO_2 should be affected by the interactions. Then, the LSPR-induced charge separation system can be utilized as a biosensor. In comparison to an optical measurement, this electrical method has the potential to achieve real-time and highly sensitive measurements for biosensing with a compact size.

A few studies regarding the utilization of the plasmon-induced photocurrent generation system as PEC biosensors to measure biomolecular interactions have been reported [22–24]. However, a quantitative measurement that can reveal the binding kinetics has not received much attention even though the kinetic parameter is indispensable to understand the binding mechanism. Moreover, both UV light as well as visible light irradiation are required to excite the semiconductor because the signal-to-noise ratio of the system was poor. Therefore, a very good signal response with a sufficient signal-to-noise ratio under visible light for real-time monitoring of molecular binding affinities and kinetics remains challenging. To overcome this problem, in this study, the photocurrent response was pursued based on the photocurrent value being enhanced by near-field coupling between the gold nanostructures with self-assembled thiol-terminated biotin (TTB) and streptavidin-modified gold nanoparticles (STA-AuNPs). The gold-nanostructured TiO_2 photoelectrode was prepared by sputtering a gold film onto a TiO_2 substrate followed by high-temperature annealing processes [16]. Gold nanoislands (AuNIs) were successfully formed on the TiO_2 photoelectrode after annealing. The TTB was used for direct binding to the AuNIs due to the extremely strong Au–S bond [25–28]. The Au–S bond has good selectivity to prevent interactions with other functional groups and good resistance to acid, alkali, and external forces. The STA-AuNPs were selected as a model target due to its specific interaction with biotin and the enhancement ability of the photocurrent generation induced by the AuNPs. The distance between the AuNIs and the AuNPs should be approximately a few nanometers due to binding of TTB and STA. Therefore, strong interparticle interactions between AuNIs and AuNPs should yield intense effects on the hot-electron transfer process [29–32]. Compared to only TTB modification, remarkable photocurrent enhancement around the LSPR region was obtained after STA-AuNPs modification. Moreover, a good photocurrent response to different concentrations of STA-AuNPs was achieved by the three-electrode measurement system under irradiation with 600 nm monochromatic light. Furthermore, the biotin-STA association and dissociation rate constants were determined via direct real-time monitoring of the photocurrent followed by fitting the time-dependent photocurrent signal using the kinetic model for stepwise binding. This biosensing system can quantitatively detect binding of biomolecules without oxidation of organic compounds due to UV irradiation. Although this study uses a well-known TTB-STA system in order to demonstrate the proposed principle, this PEC biosensor can be applied to a real-time binding kinetic monitoring of other biomolecular interactions, such as antibody-antigen [33,34] and DNA-protein [35,36].

2. Experimental section

2.1. Materials and reagents preparation

TiO_2 (Rutile, single crystal [001] Crystal Base, 0.05 wt % niobium doped, 10 × 10 × 0.5 mm^3), which was purchased from Furuuchi Chemical, was selected as the photoelectrode in this study. TTB (HS-$(CH_2)_{11}$-NH-CO-biotin, ProChimia Co., Gdansk, Poland), STA (Jackson ImmunoResearch, PA, USA), Bovine Serum Albumin modified AuNP (BSA-AuNP, 98 nM, EM.BSA10, BBI, Cardiff, UK) and STA-AuNP (98 nM, EM.STP20, BBI, Cardiff, UK) conjugate solution were used for the bio-modifications. 0.098 nM, 0.29 nM, 0.98 nM, 2.9 nM, 9.8 nM and 29 nM STA-AuNP solutions were also prepared using a mixture of pristine 98 nM STA-AuNP and a TBS buffer solution (Wako Pure Chemical Industries, Ltd.). 5 mg of TTB were dissolved in 5 mL of 2-propanol with ultrasonication in a sealed vessel. STA in a TBS buffer solution was also prepared as a control experiment for the STA-AuNPs.

2.2. AuNIs/TiO_2 photoelectrode preparation and modifications

The TiO_2 substrate was sequentially rinsed with acetone, methanol, and deionized water in an ultrasonic bath for 5 min each and dried with compressed N_2. The gold nanoislands-loaded TiO_2 (AuNIs/TiO_2) photoelectrode was fabricated by depositing a 3 nm Au film on the surface of the TiO_2 substrate with subsequent annealing at 800 °C for 1 h under a N_2 atmosphere. The AuNIs/TiO_2 sample was immersed into a TTB solution in a sealed vessel for 2 h at room temperature and sequentially rinsed with 2-propanol and deionized water in an ultrasonic bath for 5 min each and dried by compressed N_2. The same method was employed to process the STA-AuNPs modifications but using 24 h to ensure complete biotin-STA combination. After STA-AuNPs modification, the samples were cleaned by immersion into deionized water followed by shaking by hand for 30 s. The samples were cleaned thrice to ensure minimum physical adsorption of the STA-AuNPs. The nonspecific adsorptions of STA-AuNPs and other protein molecules to AuNIs with and without TTB modification were negligible in our system (Figs. S1 and S2). In addition to the STA-AuNPs, the STA without AuNPs modification was also introduced as a control experiment (Fig. S3). The extinction spectra were measured before and after modification using a spectrometer (PMA-11, Hamamatsu Photonics) equipped with an optical microscope (BX-51, Olympus)

Please cite this article in press as: J. Guo, et al., Plasmon-induced photoelectrochemical biosensor for *in situ* real-time measurement of biotin-streptavidin binding kinetics under visible light irradiation, Analytica Chimica Acta (2017), http://dx.doi.org/10.1016/j.aca.2016.12.025

via an optical fiber. The morphologies of the samples were observed by field-emission scanning electron microscopy (FE-SEM, JSM-6700FT, JEOL) with a maximum resolution of 1 nm at an electron acceleration voltage of 15 kV.

2.3. PEC measurement

An In−Ga alloy (4:1 in weight ratio) film and a thin layer of silver were pasted on the back of the AuNIs/TiO_2 substrate to achieve good Ohmic contact and electron conductivity. A platinum wire (counter electrode), a saturated calomel electrode (reference electrode) and AuNIs/TiO_2 (working electrode) were connected to an electrochemical analyzer (ALS/CH Instruments 852C, ALS) to create a three-electrode system. An aqueous $KClO_4$ (0.1 mol/L) solution was used as the supporting electrolyte solution. A xenon lamp as a light source (Model 66870, Newport), bandpass filters with a full width at half-maximum (fwhm) of less than 15 nm were employed to obtain the IPCE action spectrum, and the working potential was set to +0.3 V versus the reference electrode during the photocurrent measurement. The power density of the light source at 600 nm monochromatic light is 2.06 mW. The AuNIs/TiO_2 without modification, with TTB modification, and STA/STA-AuNPs modification were measured separately to detect the whole photocurrent change in the visible range. *In situ* measurement of the biotin-STA association was achieved by step-by-step injection of different amounts of pristine 98 nM STA-AuNP solution (0.15 μL, 0.15 μL, 0.3 μL, 0.6 μL, 1.2 μL, 2.4 μL, 4.8 μL, 4.8 μL, 4.8 μL, and 4.8 μL) into the reaction chamber that was equipped with a TTB-modified AuNIs/TiO_2 electrode and 150 μL of a $KClO_4$ solution. For *in situ* measurement, a platinum wire was employed as a quasi-reference electrode due to the special reaction chamber design.

2.4. Kinetics analysis

Based on the SEM measurements of different STA-AuNP concentrations modified TTB modified AuNIs (TTB-AuNIs), we speculate that stepwise binding between TTB-AuNIs and STA-AuNPs exists as follows: $A + B \leftrightarrows AB$, $AB + A \leftrightarrows A_2B$, where A and B represent STA-AuNP and TTB-AuNI, respectively. AB and A_2B are the newly formed products in the stepwise binding pathway. The real-time sensorgram characteristics of the photocurrent evolution at different concentrations of STA-AuNP as a function of time were solved numerically utilizing software (SimFit, 32 bit, Version 7.1.5 http://www.simfit.org.uk/).

3. Results and discussion

3.1. Extinction and PEC measurements before and after biomolecule modified AuNIs/TiO_2

Fig. 1a shows the extinction spectra of STA-AuNPs (black), AuNIs/TiO_2 photoelectrode (red) after TTB modification (blue) as well as the subsequent STA-AuNPs modification (magenta). The LSPR peaks of STA-AuNPs and the AuNIs/TiO_2 are located around 530 nm and 600 nm, respectively. The 600 nm LSPR peak of AuNIs/TiO_2 is due to the large refractive index of TiO_2 and also can be verified by finite-difference time-domain (FDTD) simulations (Fig. S4). The LSPR peak of AuNIs/TiO_2 exhibited a redshift, and the extinction value increased after TTB and STA-AuNPs modifications, demonstrating the successful bindings of TTB on AuNIs and STA-AuNPs on TTB. Fig. 1b shows the *I-t* curves with irradiation of monochromatic light at 600 nm (LSPR region) of TiO_2 (black), AuNIs/TiO_2 (red) and after each condition. The photocurrent of AuNIs/TiO_2 is more than 100 times larger than that of TiO_2, demonstrating the significance of plasmon-induced photocurrent generation. The photocurrent was weakened with the TTB modification. However, the photocurrent was enhanced after both TTB and STA-AuNPs modifications. The result indicated that the TTB molecules may prevent water molecules from acting as electron donors. However, the interparticle interactions between AuNIs and AuNPs can enhance the photoactivity of the electrode after modification of STA-AuNPs (Fig. S5). Additionally, spikes appeared in the photocurrents in Fig. 1b when the light turned on for AuNIs/TiO_2 sample with irradiation of 600 nm light. Although the origin of the spike of the photocurrents is still under investigation, there is a possibility that the charging current on the surface of the gold attribute the spike of the photocurrent. The spike disappeared after modification of TTB and STA-AuNPs. These phenomena also can be explained by the change of the gold surface due to the coating with organic molecules. The spikes do not affect the IPCE in Fig. 1c because the IPCE values were calculated from quasi-steady-state current. A control experiment (Fig. S3) demonstrated that the STA without the AuNPs did not enhance the photocurrent of the TTB-modified AuNIs/TiO_2 electrode. The entire IPCE action spectra change is shown in Fig. 1c. In comparison to only the TTB modification, enhancement was observed after both the TTB and STA-AuNPs modifications over the entire LSPR region. This result indicates that the TTB-AuNIs/TiO_2 photoelectrode is sensitive to the STA-AuNPs modifications. The detailed mechanism that explains these phenomena will be discussed in a later section.

3.2. In situ measurement of STA-AuNPs

A stepwise increase in the photocurrent value was observed under irradiation with 600 nm light after each injection of STA-AuNPs, as shown in Fig. 2a. The sudden drop of the photocurrent response during the injection (only few seconds), which is due to a portion of the light being blocked by the needle of the microsyringe induced by the special design of extremely small reaction chamber, was delated to be depicted by a clearer representation (the original *in situ* photocurrent response was shown in Fig. S6). The photocurrent finally becomes saturated, indicating that the TTB binding sites were nearly occupied by STA-AuNPs. Fig. 2b shows the normalized photocurrent enhancement as a function of different concentrations of STA-AuNP. The normalized photocurrent enhancement at each concentration was calculated by $\Delta i/\Delta i_{max}$, where Δi and Δi_{max} are the photocurrent increase at the concentration and the maximum value of the photocurrent increase, respectively.

3.3. SEM measurement and proposed mechanism

Fig. 3 shows proposed schematic diagrams and the corresponding SEM images after modification with different concentrations of STA-AuNP. As shown in Fig. 3b, one-to-one bindings between TTB-AuNI and STA-AuNP were predominately observed at a concentration of 0.98 nM compared to that for only AuNIs, as shown in Fig. 3a. Multi-STA-AuNPs binding to one AuNI appears to be limited. However, multi-STA-AuNPs binding to one AuNI increased at a concentration of 2.9 nM, as shown in Fig. 3c. 98 nM STA-AuNPs modification shows lots of examples of multi-STA-AuNPs binding to one AuNI (Fig. S7). The proposed mechanism is described below. For the AuNIs/TiO_2 photoelectrode, the LSPR-induced charge separation will be activated under visible light irradiation. In this case, the water molecules act as electron donors, and the electrons from the AuNIs inject to the conduction band of TiO_2. After TTB modification, the AuNI surface was covered by layers of TTB molecules. The TTB molecules may prevent the water molecules from acting as electron donors for photocurrent generation. Therefore, the photocurrent decreases. For the lower concentration

Please cite this article in press as: J. Guo, et al., Plasmon-induced photoelectrochemical biosensor for *in situ* real-time measurement of biotin-streptavidin binding kinetics under visible light irradiation, Analytica Chimica Acta (2017), http://dx.doi.org/10.1016/j.aca.2016.12.025

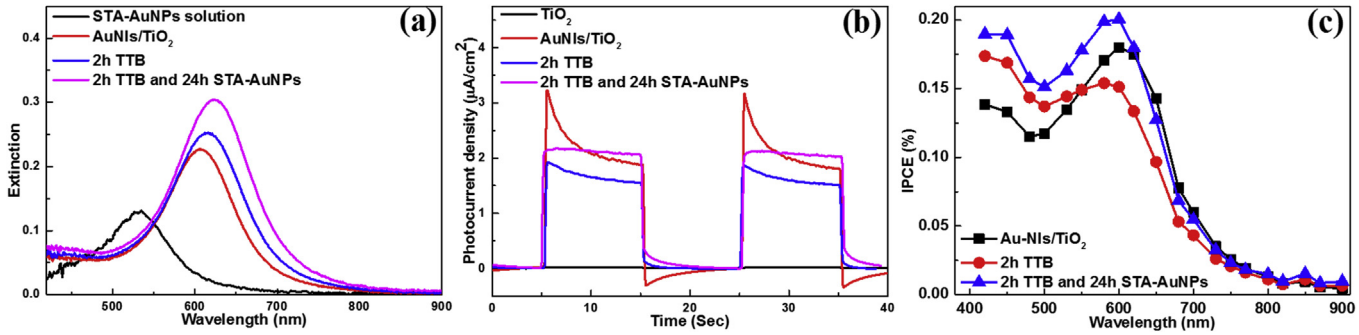

Fig. 1. (a) Extinction spectra of STA-AuNPs (black), AuNIs/TiO_2 photoelectrode (red), after TTB modification (blue) and subsequent STA-AuNPs modification (magenta). (b) The photocurrent response under irradiation with 600 nm monochromatic light of TiO_2 (black), AuNIs/TiO_2 photoelectrode (red), after TTB modification (blue) and subsequent STA-AuNPs modification (magenta). (c) The corresponding IPCE action spectral evolution of the AuNIs/TiO_2 photoelectrode. (For interpretation of the references to colour in this figure legend, the reader is referred to the web version of this article.)

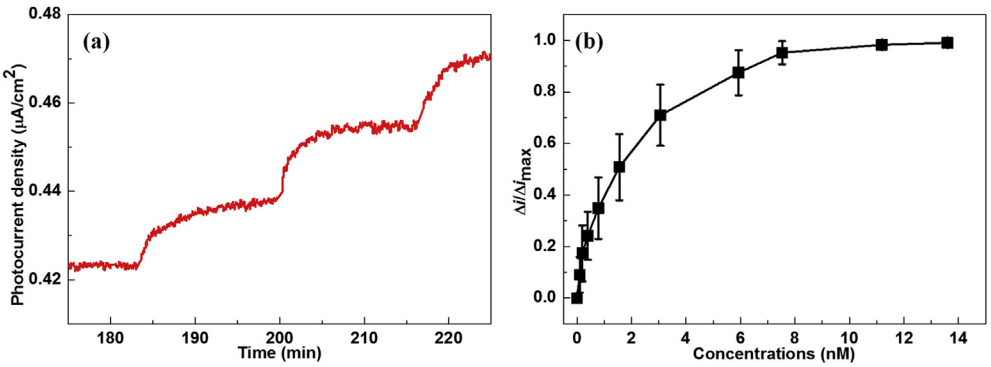

Fig. 2. (a) Representative *in situ* photocurrent response to different concentrations of STA-AuNP under irradiation with 600 nm monochromatic light. (b) Normalized photocurrent enhancement as a function of different concentrations of STA-AuNP. The error bars indicate the standard deviation of five replicate measurements.

region of STA-AuNPs modification, the binding between TTB-AuNIs and STA-AuNPs primarily occurs in a one-to-one fashion. The introduced strong interparticle interactions between AuNPs and AuNIs promote enhanced photocurrent generation. For the higher concentration region, multi-STA-AuNPs connect to one AuNI. When the bindings between TTB-AuNIs and STA-AuNPs reach a maximum, the photocurrent becomes saturated.

3.4. Kinetics measurement

The binding kinetics between TTB-AuNIs and STA-AuNPs were analyzed by utilizing a time-dependent model that represents a

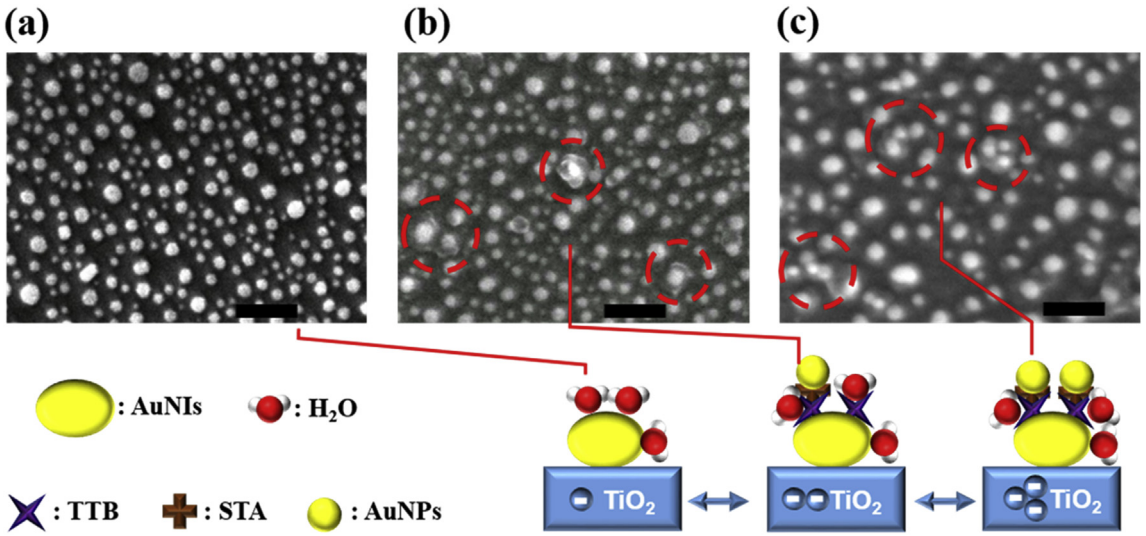

Fig. 3. SEM images of AuNIs without modification (a) and after TTB modification and subsequent 0.98 nM (b) and 2.9 nM (c) STA-AuNPs modifications. The scale bars represent 100 nm. The schematic diagrams show the binding mode that corresponds to the SEM image. The SEM images were processed by GIMP software (https://www.gimp.org/) to get greater clarity and resolution because the original SEM images were blurred due to the organic molecules.

Please cite this article in press as: J. Guo, et al., Plasmon-induced photoelectrochemical biosensor for *in situ* real-time measurement of biotin-streptavidin binding kinetics under visible light irradiation, Analytica Chimica Acta (2017), http://dx.doi.org/10.1016/j.aca.2016.12.025

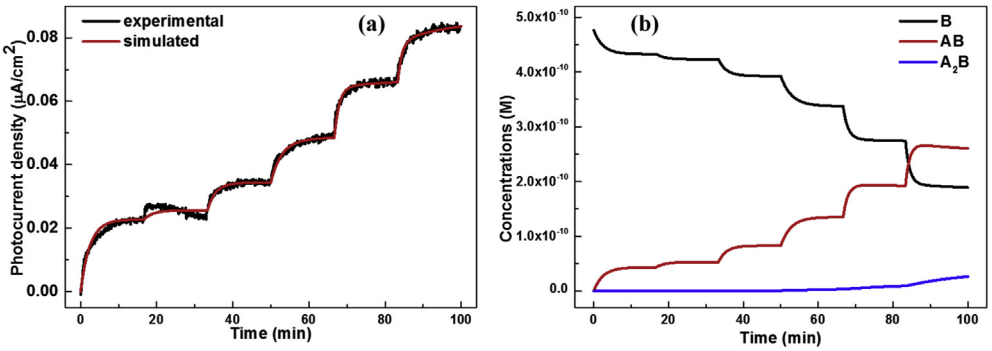

Fig. 4. (a) Experimental and simulated photocurrents as a function of time at different concentrations of STA-AuNP. (b) The simulated evolutions of B, AB, and A_2B as a function of time at different concentrations of STA-AuNP.

stepwise reaction:

$$A + B \underset{k_{-1}}{\overset{k_1}{\rightleftarrows}} AB \quad (1a)$$

$$A + AB \underset{k_{-2}}{\overset{k_2}{\rightleftarrows}} A_2B \quad (1b)$$

where A, B, AB and A_2B represent the STA-AuNPs, TTB-AuNIs, newly formed complex at the first binding step (one STA-AuNP to one TTB-AuNI) and the complex second binding step (two STA-AuNPs to one TTB-AuNI), respectively. The relationship between the photocurrent enhancement and AB and A_2B was assumed to be:

$$\Delta i = \alpha[AB] + \beta[A_2B] \quad (2)$$

where Δi is the increase in the photocurrent, α and β represent the contributions to the photocurrent enhancement of AB and A_2B, respectively, and [AB] and [A_2B] represent the concentrations of AB and A_2B, respectively. The coupled differential equations arising from Eqs. (1) and (2) were solved numerically using the SimFit software (Supporting Information). The initial concentrations of A and B need to be known at each injection. The concentration of A can be easily calculated from the specification. The calculation of initial concentration of B is shown in the supporting information and Fig. S8.

Fig. 4a shows the experimental (black) and simulated (red) photocurrents as a function of time at different concentrations of STA-AuNP (a few points in the high concentration region are unavailable due to a lack of enhancement), and these results are in good agreement (Detailed information related to the fitting results is shown in Supporting Information). Fig. 4b shows the corresponding evolutions of the reactant (B) and products (AB and A_2B) at different concentrations of A (The evolution of A is not shown due to the successive injections). As shown in Fig. 4b, for the first four concentrations of A, the AB product is predominately formed, and the A_2B product formation is negligibly small (one notable point is that AB always increases during each injection). The result demonstrates that the binding between TTB-AuNIs and STA-AuNPs was nearly one-to-one binding in the lower concentration region. However, for the last two concentrations, the A_2B product increases to the same order as AB, demonstrating that binding between multi-STA-AuNPs and one AuNI is a competitive one-to-one binding in the higher concentration region (AB increases at first and then decreases during each injection). These results are in good agreement with the SEM measurement and confirm our hypothesis (Fig. 3).

Table 1 shows the association and dissociation rate constants as well as related kinetic parameters at different concentrations of STA-AuNP. The association rate constant of the first binding step (k_1) was two orders faster than that of the second binding step (k_2). The binding of the second STA-AuNP was retarded by steric hindrance [37] due to initial binding between STA-AuNP and TTB-AuNI. It is important to note that k_1 and k_2 exhibit a small concentration dependence on STA-AuNP. This phenomenon can also be explained by the steric hindrance of the STA-AuNP bound to the adjacent TTB-AuNI. The relative thermodynamic binding constants of two binding steps can be calculated as follows: $K_{a,\,surf1} = k_1/k_{-1} = (7.67 \pm 0.73) \times 10^8\ M^{-1}$, $K_{a,\,surf2} = k_2/k_{-2} = (5.54 \pm 0.14) \times 10^7\ M^{-1}$, and these values are smaller than that reported for biotin-STA association ($1 \times 10^{11}\ M^{-1}$) [8] but larger than another reported value $3 \times 10^6\ M^{-1}$ [38].

4. Conclusions

In summary, we have successfully developed a surface plasmon-induced visible light-responsive PEC biosensor using a TTB-modified AuNIs/TiO_2 photoelectrode for *in situ* real-time measurement of the biotin-STA binding kinetics. The interparticle interactions between the AuNIs and the introduced AuNPs enhanced the photocurrent generation. Good concentration dependence of the photocurrent response was observed under irradiation with 600 nm monochromatic light with high sensitivity, which prevents

Table 1
Association and dissociation rate constants and related kinetic parameters at different concentrations of STA-AuNP.

Concentration of STA-AuNP (M)	9.86×10^{-11}	1.966×10^{-10}	3.926×10^{-10}	7.823×10^{-10}	1.553×10^{-9}	3.057×10^{-9}	Average
k_1 ($M^{-1}s^{-1}$)	6.43×10^6	4.11×10^6	3.60×10^6	2.29×10^6	3.68×10^6	3.00×10^6	$(3.85 \pm 1.41) \times 10^6$
k_{-1} (s^{-1})	3.51×10^{-3}	4.70×10^{-3}	5.24×10^{-3}	3.65×10^{-3}	7.03×10^{-3}	5.96×10^{-3}	$(5.02 \pm 1.36) \times 10^{-3}$
k_2 ($M^{-1}s^{-1}$)	5.42×10^4	5.42×10^4	5.42×10^4	5.91×10^4	5.13×10^4	5.09×10^4	$(5.40 \pm 0.29) \times 10^4$
k_{-2} (s^{-1})	9.75×10^{-4}	9.75×10^{-4}	9.75×10^{-4}	9.25×10^{-4}	9.99×10^{-4}	1.00×10^{-3}	$(9.75 \pm 0.27) \times 10^{-4}$
α	5.23×10^8	3.01×10^8	2.85×10^8	2.47×10^8	2.64×10^8	1.66×10^8	$(2.98 \pm 1.20) \times 10^8$
β	4.09×10^8	4.08×10^8	4.08×10^8	4.50×10^8	3.82×10^8	3.75×10^8	$(4.05 \pm 0.26) \times 10^8$

Please cite this article in press as: J. Guo, et al., Plasmon-induced photoelectrochemical biosensor for *in situ* real-time measurement of biotin-streptavidin binding kinetics under visible light irradiation, Analytica Chimica Acta (2017), http://dx.doi.org/10.1016/j.aca.2016.12.025

UV light-induced decomposition of organic molecules (i.e., both the receptors and targets). Moreover, direct investigation of the binding kinetics of the biotin-STA association can be achieved by real-time monitoring of the PEC sensing characteristics. The stepwise binding model between STA-AuNPs and TTB-AuNIs is consistent with the experimental results. The surface-confined thermodynamic binding constant can be calculated. The proposed biosensor that is based on plasmon-induced photocurrent generation is useful for both thermodynamic and kinetic analyses of interactions of various biomolecules and expected to allow the facile miniaturization of the instrument. This method opens a new avenue for the specific electrical detection of biomolecular interactions and real-time binding kinetic measurements.

Acknowledgments

We gratefully acknowledge financial support from JSPS KAKENHI Grant Nos. JP23225006, JP15H00856, JP15K17438, JP15H01073, and JP15K04589, the Nanotechnology Platform (Hokkaido University), and Nano-Macro Materials, Devices and System Research Alliance of MEXT.

Appendix B. Supplementary data

Supplementary data related to this article can be found at http://dx.doi.org/10.1016/j.aca.2016.12.025.

References

[1] K.M. Mayer, J.H. Hafner, Localized surface plasmon resonance sensors, Chem. Rev. 111 (2011) 3828–3857.
[2] M.C. Estevez, M.A. Otte, B. Sepulveda, L.M. Lechuga, Trends and challenges of refractometric nanoplasmonic biosensors: a review, Anal. Chim. Acta 806 (2014) 55–73.
[3] S.W. Zeng, D. Baillargeat, H.P. Ho, K.T. Yong, Nanomaterials enhanced surface plasmon resonance for biological and chemical sensing applications, Chem. Soc. Rev. 43 (2014) 3426–3452.
[4] A.J. Haes, R.P. Van Duyne, Preliminary studies and potential applications of localized surface plasmon resonance spectroscopy in medical diagnostics, Expert Rev. Mol. Diagn. 4 (2004), 1473–7159.
[5] U. Kreibig, M. Vollmer, Optical Properties of Metal Clusters, Springer, Berlin, 1995.
[6] P. Mulvaney, Surface plasmon spectroscopy of nanosized metal particles, Langmuir 12 (1996) 788–800.
[7] G.V. Hartland, Optical studies of dynamics in noble metal nanostructures, Chem. Rev. 111 (2011) 3858–3887.
[8] A.J. Haes, R.P. Van Duyne, A nanoscale optical biosensor: sensitivity and selectivity of an approach based on the localized surface plasmon resonance spectroscopy of triangular silver nanoparticles, J. Am. Chem. Soc. 124 (2002) 10596–10604.
[9] H.M. Kim, S.M. Jin, S.K. Lee, M.G. Kim, Y.B. Shin, Detection of biomolecular binding through enhancement of localized surface plasmon resonance (LSPR) by gold nanoparticles, Sensors 9 (2009) 2334–2344.
[10] N. Nath, A. Chilkoti, A colorimetric gold nanoparticle sensor to interrogate biomolecular interactions in real time on a surface, Anal. Chem. 74 (2002) 504–509.
[11] N. Nath, A. Chilkoti, Label-free biosensing by surface plasmon resonance of nanoparticles on glass: optimization of nanoparticle size, Anal. Chem. 76 (2004) 5370–5378.
[12] G.L. Zhao, H. Kozuka, T. Yoko, Sol-gel preparation and photoelectrochemical properties of TiO_2 films containing Au and Ag metal particles, Thin Solid Films 277 (1996) 147–154.
[13] Y. Tian, T. Tatsuma, Mechanisms and applications of plasmon-induced charge separation at TiO_2 films loaded with gold nanoparticles, J. Am. Chem. Soc. 127 (2005) 7632–7637.
[14] Y. Nishijima, K. Ueno, Y. Yokota, K. Murakoshi, H. Misawa, Plasmon-assisted photocurrent generation from visible to near-infrared wavelength using a Au-nanorods/TiO_2 electrode, J. Phys. Chem. Lett. 1 (2010) 2031–2036.
[15] Y. Nishijima, K. Ueno, Y. Kotake, K. Murakoshi, H. Inoue, H. Misawa, Near-infrared plasmon-assisted water oxidation, J. Phys. Chem. Lett. 3 (2012) 1248–1252.
[16] X. Shi, K. Ueno, N. Takabayashi, H. Misawa, Plasmon enhanced photocurrent generation and water oxidation with a gold nanoisland loaded titanium dioxide photoelectrode, J. Phys. Chem. C 117 (2012) 2494–2499.
[17] C. Clavero, Plasmon-induced hot-electron generation at nanoparticle/metal-oxide interfaces for photovoltaic and photocatalytic devices, Nat. Photonics 8 (2014) 95–103.
[18] Y.Q. Zhong, K. Ueno, Y. Mori, X. Shi, T. Oshikiri, K. Murakoshi, H. Inoue, H. Misawa, Plasmon-assisted water splitting using two sides of the same $SrTiO_3$ single-crystal substrate: conversion of visible light to chemical energy, Angew. Chem. Int. Ed. 53 (2014) 10350–10354.
[19] T. Oshikiri, K. Ueno, H. Misawa, Plasmon-induced ammonia synthesis through nitrogen photofixation with visible light irradiation, Angew. Chem. Int. Ed. 126 (2014) 9802–9805.
[20] X.M. Zhang, Y.L. Chen, R.S. Liu, D.P. Tsai, Plasmonic photocatalysis, Rep. Prog. Phys. 76 (2013), 046401 (41pp).
[21] A. Tanaka, Y. Nishino, S. Sakaguchi, T. Yoshikawa, K. Imamura, K. Hashimoto, H. Kominami, Functionalization of a plasmonic Au/TiO_2 photocatalyst with an Ag co-catalyst for quantitative reduction of nitrobenzene to aniline in 2-propanol suspensions under irradiation of visible light, Chem. Commun. 49 (2013) 2551–2553.
[22] A.W. Zhu, Y.P. Luo, Y. Tian, Plasmon-induced enhancement in analytical performance based on gold nanoparticles deposited on TiO_2 film, Anal. Chem. 81 (2009) 7243–7247.
[23] W.W. Zhao, C.Y. Tian, J.J. Xu, H.Y. Chen, The coupling of localized surface plasmon resonance-based photoelectrochemistry and nanoparticle size effect: towards novel plasmonic photoelectrochemical biosensing, Chem. Commun. 48 (2012) 895–897.
[24] P.M. Da, W.J. Li, X. Lin, Y.C. Wang, J. Tang, G.F. Zheng, Surface plasmon resonance enhanced real-time photoelectrochemical protein sensing by gold nanoparticle decorated TiO_2 nanowires, Anal. Chem. 86 (2014) 6633–6639.
[25] R.G. Nuzzo, B.R. Zegarski, L.H. Dubois, Fundamental studies of the chemisorption of organosulfur compounds on Au (111). Implications for molecular self-assembly on gold surfaces, J. Am. Chem. Soc. 109 (1987) 733–740.
[26] C.D. Bain, E.B. Troughton, Y.T. Tao, J. Evall, G.M. Whitesides, R.G. Nuzzo, Formation of monolayer films by the spontaneous assembly of organic thiols from solution onto gold, J. Am. Chem. Soc. 111 (1989) 321–335.
[27] H. Sellers, A. Ulman, Y. Shnidman, E.E. James, Structure and binding of alkanethiolates on gold and silver surfaces: implications for self-assembled monolayers, J. Am. Chem. Soc. 115 (1993) 9389–9401.
[28] M. Brust, M. Walker, D. Bethell, D.J. Schiffrin, R. Whyman, Synthesis of thiol-derivatised gold nanoparticles in a two-phase liquid-liquid system, J. Chem. Soc. Chem. Commun. (1994) 801–802.
[29] W. Rechberger, A. Hohenau, A. Leitner, J.R. Krenn, B. Lamprecht, F.R. Aussenegg, Optical properties of two interacting gold nanoparticles, Opt. Commun. 220 (2003) 137–141.
[30] K.G. Sujit, P. Tarasankar, Interparticle coupling effect on the surface plasmon resonance of gold nanoparticles: from theory to applications, Chem. Rev. 107 (2007) 4797–4862.
[31] N.J. Halas, S. Lal, W.S. Chang, S. Link, P. Nordlander, Plasmons in strongly coupled metallic nanostructures, Chem. Rev. 111 (2011) 3913–3961.
[32] T. Kawawaki, Y. Takahashi, T. Tatsuma, Enhancement of dye-sensitized photocurrents by gold nanoparticles: effects of plasmon coupling, J. Phys. Chem. C 117 (2013) 5901–5907.
[33] A.J. Haes, L. Chang, W.L. Klein, R.P. Van Duyne, Detection of a biomarker for Alzheimer's disease from synthetic and clinical samples using a nanoscale optical biosensor, J. Am. Chem. Soc. 127 (2005) 2264–2271.
[34] K.M. Mayer, S. Lee, H. Liao, B.C. Rostro, A. Fuentes, P.T. Scully, C.L. Nehl, J.H. Hafner, A label-free immunoassay based upon localized surface plasmon resonance of gold nanorods, ACS Nano 4 (2008) 687–692.
[35] Y.L. Zhou, Z.N. Xu, M. Wang, B. Sun, H.S. Yin, S.Y. Ai, DNA methyltransferase activity assay based on visible light-activated photoelectrochemical biosensor, Biosens. Bioelectron. 53 (2014) 263–267.
[36] W.W. Zhao, J.J. Xu, H.Y. Chen, Photoelectrochemical DNA biosensors, Chem. Rev. 114 (2014) 7421–7441.
[37] T. Buranda, G.M. Jones, J.P. Nolan, J. Keij, G.P. Lopez, L.A. Sklar, Ligand receptor dynamics at streptavidin-coated particle surfaces: a flow cytometric and spectrofluorimetric study, J. Phys. Chem. B 103 (1999) 3399–3410.
[38] T. Arai, P.K.R. Kumar, C. Rockstuhl, K. Awazu, J. Tominaga, An optical biosensor based on localized surface plasmon resonance of silver nanostructured films, J. Opt. A Pure Appl. Opt. 9 (2007) 699–703.

Please cite this article in press as: J. Guo, et al., Plasmon-induced photoelectrochemical biosensor for *in situ* real-time measurement of biotin-streptavidin binding kinetics under visible light irradiation, Analytica Chimica Acta (2017), http://dx.doi.org/10.1016/j.aca.2016.12.025